PCCP

PAPER

View Article Online
View Journal | View Issue

Cite this: *Phys. Chem. Chem. Phys.*, 2014, **16**, 2062

Highly conductive poly(3,4-ethylenedioxypyrrole) and poly(3,4-ethylenedioxythiophene) enwrapped Sb_2S_3 nanorods for flexible supercapacitors†

B. Narsimha Reddy,[a] Melepurath Deepa*[a] and Amish G. Joshi[b]

Received 21st August 2013,
Accepted 18th November 2013

DOI: 10.1039/c3cp53554a

www.rsc.org/pccp

Composites of poly(3,4-ethylenedioxypyrrole) or PEDOP and poly(3,4-ethylenedioxythiophene) or PEDOT enwrapped Sb_2S_3 nanorods have been synthesized for the first time for use as supercapacitor electrodes. Hydrothermally synthesized Sb_2S_3 nanorods, several microns in length and 50–150 nm wide, offer high surface area and serve as a scaffold for coating conducting polymers, and are a viable alternative to carbon nanostructures. Fibrillar morphologies are achieved for the PEDOP–Sb_2S_3 and PEDOT–Sb_2S_3 films in contrast to the regular granular topologies attained for the neat polymers. The remarkably high nano-scale (~5 S cm^{-1}) conductivity of the Sb_2S_3 nanorods enables facile electron transport in the composites. We constructed asymmetric supercapacitors using the neat polymer or composite and graphite as electrodes. High specific capacitances of 1008 F g^{-1} and 830 F g^{-1} (at 1 A g^{-1}), enhanced power densities (504 and 415 W kg^{-1}) and excellent cycling stability (88 and 85% capacitance retention at the end of 1000 cycles) are delivered by the PEDOP–Sb_2S_3 and PEDOT–Sb_2S_3 cells relative to the neat polymer cells. A demonstration of a light emitting diode illumination using a light-weight, flexible, supercapacitor fabricated with PEDOP–Sb_2S_3 and carbon-fiber cloth shows the applicability of Sb_2S_3 enwrapped conducting polymers as sustainable electrodes for ultra-thin supercapacitors.

1. Introduction

Redox supercapacitors based on conducting polymer composites are arousing enormous research interest for use as electrodes in high power energy storage devices such as electric vehicles and portable electronic devices. Supercapacitors work in tandem with batteries to provide high peak power and to increase the operational lifetime of batteries.[1–3] A redox supercapacitor relies on the pseudocapacitive nature of the electroactive material (like a conducting polymer) and stores energy faradaically, which involves mass transfer (ions and electrons) at the conducting polymer/electrolyte and current collector/conducting polymer interfaces.[4,5] Conducting polymers offer many advantages: they can be easily switched between reduced (dedoped) and oxidized (doped) states, they are cheap, offer low toxicity and can be easily prepared in bulk or film forms at room temperature. Further, by inclusion of a chemically compatible electronically conducting nanostructured moiety (such as multi-walled carbon nanotubes) along with the conducting polymer, the large surface area of the nanotubes enables a large mass loading of the conducting polymer, which effectively leads to a high capacitance.[6,7] In a pristine conducting polymer electrode based cell, owing to the poor accessibility of the electrolyte to the internal redox active sites on the polymer, a consequence of the compact granular polymer morphology, the electroactive material remains largely under-utilized and therefore the capacitances are not very high.[8] Until now, most efforts have been devoted to creating conducting polymer nanocomposites with either electronically conductive carbon nanostructures such as graphene, carbon nanotubes, carbon fibers[9–11] or by use of a complementary pseudocapacitive transition metal oxide like RuO_2, MnO_2, Co_3O_4, V_2O_5 and NiO.[12–16] In a carbon nano-moiety-conducting polymer composite, the synergy between the ability of the polymer to store and release faradaic charge by undergoing redox reactions and the capability of the carbon nano-moiety to function as an electron conduit, thereby allowing charge storage by electrical double layer formation, translates into high capacitance and therefore high power density. The need to develop new alternate materials capable of charge storage stems from the fact that supercapacitor designs using

[a] *Department of Chemistry, Indian Institute of Technology Hyderabad, Ordnance Factory Estate, Yeddumailaram-502205, Andhra Pradesh, India. E-mail: mdeepa@iith.ac.in; Tel: +91-40-23016024*

[b] *CSIR-National Physical Laboratory, Dr K.S. Krishnan Road, New Delhi-110012, India*

† Electronic supplementary information (ESI) available: XRD patterns of Sb_2S_3, Raman spectra of Sb_2S_3, neat PEDOP and neat PEDOT, cross-sectional profiles of topography and current extracted from C-AFM images of the electrodes, C-AFM images and cross-sectional profiles of neat PEDOP and PEDOT and tabulated impedance parameters. See DOI: 10.1039/c3cp53554a

carbon nanostructures/conducting polymer composites have been exhaustively investigated and possibilities are often limited to the use of graphene or multi/single-walled carbon nanotubes or fibers. In the past, although graphene or multi/single-walled carbon nanotube enwrapped conducting polymer composites have demonstrated excellent performance characteristics, when employed as electrodes in supercapacitors, but further improving the electrical conductivity of the composite at a low cost remains a formidable challenge. Among various desirable architectures for electrodes, one-dimensional nanostructures are attractive as they offer short diffusion lengths for ions and high charge–discharge rates. For instance, a poly(aniline) fibrous structure coated with MnO_2 nanorods yielded a specific capacitance of 417 F g^{-1}.[17] Yet another study on an ultrathin flexible all-solid-state supercapacitor with carbon nanotubes–poly(aniline) or PANI nanocomposite thin films as electrodes showed a rather high specific capacitance of 350 F g^{-1} in its twisted state.[18] Another report on a novel supercapacitor with a pyrene functionalized polyfluorene as an adhesive inter-layer between poly(3,4-propylenedioxypyrrole) and single walled carbon nanotubes revealed a capacitance of 122 F g^{-1}.[19] In a previous report, flexible, uniform graphene–poly(pyrrole) composite films prepared by a pulsed electro-polymerization technique exhibited a specific capacitance of 237 F g^{-1} and a power density of 1184 W kg^{-1}.[20] It is obvious that carbon nanostructures by the virtue of large specific area endowed by their tubular or sheet like morphologies allow greater uptake of ions and also permit fast and efficient charge ingress and egress, thus manifesting in large specific capacitance and high power density.

By considering the above-mentioned factors which can boost supercapacitor performance, we fabricated, for the first time, electrodes of electrically conductive and economically viable, and less toxic antimony sulfide (Sb_2S_3) nanorods enwrapped by a conducting polymer like poly(3,4-ethylenedioxypyrrole) or PEDOP and poly(3,4-ethylenedioxythiophene) or PEDOT. For growing a conducting polymer directly with tube or wire like morphologies, generally, templates such as anodized alumina are employed and the process is cumbersome and the scalability is poor.[21] To alleviate this issue, we grew electronically conducting Sb_2S_3 nanorods, using a template free, inexpensive one-pot approach. Further oxidative electropolymerization from a medium containing the monomer and the nanorods allowed the conducting polymer chains to encapsulate the nanorods and deposit onto the current collector surface under a directed electric potential. The nanorod-like morphology and the excellent electronic conductivity of Sb_2S_3 allow this sulfide to play a role akin to carbon nanotubes in a conducting polymer composite. Sb_2S_3 nanorods offer the benefit of fast electron transfer at the nanorods/polymer interface, owing to the direct and intimate contact between the rods and the polymer. This is advantageous as the principal function of a supercapacitor is to deliver high power at a fast rate, when required. From the gamut of conducting polymers like poly(aniline), poly(pyrrole) and poly(3,4-ethylenedioxythiophene), we chose PEDOT and its pyrrole analogue PEDOP for preparing the composites, owing to their low oxidation potentials (0.3 V and 0.8 V *versus* Ag/Ag^+ respectively), good electrochemical stability of the doped states, robust response to repetitive redox cycling, low cost and scalability.[22–26] Solid state supercapacitor cells were fabricated by use of electrodes with three-dimensional networks of Sb_2S_3 nanorods enwrapped by PEDOT or PEDOP, an ionic liquid based gel as the electrolyte and electrophoretically deposited graphite as the counter electrode. The composite supercapacitors developed in the present study clearly outperform the neat polymer based supercapacitors, thus furnishing a new approach for fabricating advanced supercapacitors with high performance, inherently safe operation and long lifetime. Herein, we also highlight the construction and the outstanding performance of a PEDOP–Sb_2S_3 electrode based flexible, lightweight supercapacitor cell, with a carbon-fiber cloth as the current collector, wherein the distensibility, low weight and the ultra-thin architecture of the cell demonstrate the enormous practical significance of the composite, thus illustrating the promise the conductive Sb_2S_3 nanorods show as scaffolds for a plethora of electroactive materials.

2. Experimental

2.1. Chemicals

3,4-Ethylenedioxypyrrole (EDOP), 3,4-ethylenedioxythiophene (EDOT), poly(methylmethacrylate) (PMMA), sodium borohydride ($NaBH_4$), sulfur and graphite were procured from Sigma-Aldrich and used as received. 1-Butyl-3-methyl-imidazolium tris(pentafluoroethyl)trifluorophosphate ($BuMeIm^+[(C_2F_5)_3(PF_3)]^-$), antimony chloride ($SbCl_3$), ethylene glycol, isopropanol and acetone were purchased from Merck chemicals. Ultrapure water (resistivity $\sim$ 18.2 MΩ cm) was obtained through a Millipore Direct-Q3 UV system. SnO_2:F (FTO) coated glass substrates with a sheet resistance of about 14 Ω sq^{-1} were procured from Pilkington, washed with soap solution, flushed with copious amounts of distilled water and cleaned with acetone prior to use. A carbon fiber cloth of 3 mm thickness was purchased from Alibaba Pvt. Ltd.

2.2. Synthesis of Sb_2S_3 nanorods

$SbCl_3$ (0.25 g) was dissolved in ultrapure water (30 mL) and stirred for 10 min, followed by addition of ethylene glycol (30 mL) at room temperature. After stirring for another 10 min, sulfur (0.1 g) and $NaBH_4$ (0.3 g) were added slowly. The mixture was stirred for another 30 min, transferred to an autoclave of 100 mL capacity and heated for 12 h at 180 °C. A black precipitate was obtained, which was filtered and washed with deionized water and then dried at 60 °C. The resulting Sb_2S_3 nanorods were stored in air.

2.3. Fabrication of electrodes and devices

EDOP (0.1 M) and EDOT (0.1 M) monomer solutions were prepared in acetonitrile (30 mL) separately, 0.1 M 1-butyl-3-methyl-imidazolium tris(pentafluoroethyl)trifluorophosphate was used as the dopant ion source in each case. SnO_2:F (FTO) coated glass or carbon fiber cloth (of area 1 × 2 cm^2) was employed as the working electrode and a Pt sheet was used as the counter electrode and Ag/AgCl/KCl was used as the

reference electrode. Blue colored PEDOT and bluish-black PEDOP films were obtained under potentiostatic conditions at room temperature in chronoamperometric mode by application of +1.5 V to the working electrode for 500 s. The Sb_2S_3 nanorods (1.5 g) were added to the monomer bath and the solution was sonicated for 30 min and the same procedure was repeated to yield PEDOP–Sb_2S_3 and PEDOT–Sb_2S_3 films.

A dispersion of graphite (0.1 g) in ethanol (30 mL) was prepared by ultrasonication for 15 min and using a two electrode configuration with FTO coated glass or carbon fiber cloth, graphite coatings were obtained on one of the electrodes upon application of a constant potential of 20 V for 5 min using a Tarsons MC-01 electrophoresis power supply. Graphite electrodes have been labeled as Gr in this study. A quasi-solid polymer electrolyte was synthesized by dissolving PMMA (1 g) in the ionic liquid: ($BuMeIm^+[(C_2F_5)_3(PF_3)]^-$) (4 g) by continuous stirring at 80 °C for 5–6 h until a transparent viscous gel was obtained which had little flow properties when cooled to room temperature. An acrylic tape of 0.5 mm thickness was employed as the spacer and was applied along the four edges of the active electrode, the electrolyte was filled in the cavity using a glass rod and heated in a vacuum oven at 50 °C until a bubble free electrolyte layer was obtained. The counter electrode (Gr) was then pressed upon this assembly and the whole configuration was held together using binder clips and placed in an online vacuum oven for 1 h. The edges were finally sealed with an epoxy. Asymmetric cells with either FTO coated glass or carbon fiber cloth as current collectors were obtained with the following configurations: PEDOP-Gr, PEDOP–Sb_2S_3-Gr, PEDOT-Gr and PEDOT–Sb_2S_3-Gr.

2.4. Instrumental methods

X-ray photoelectron spectroscopy (XPS) was carried out using a Perkin Elmer 1257 model operating at a base pressure of $\sim 4.2 \times 10^{-8}$ Torr (100 Watt, 15 KV) with a non-monochromatized Mg Kα line at 1253.6 eV, an analyzer pass energy of 60 eV, and a hemispherical sector analyzer capable of 25 meV resolution. The overall instrumental resolution was about 0.3 eV. The core level spectra were deconvoluted using a non-linear iterative least squares Gaussian fitting procedure. For all fitting multiplets, the FWHMs were fixed accordingly. Corrections due to charging effects were taken care of by using C(1s) as an internal reference and the Fermi edge of a gold sample. Jandel Peak FitTM (version 4.01) program was used for the analyses. Absorption spectra were measured on a Shimadzu UV-visible-NIR 3600 spectrophotometer. X-ray diffraction patterns were recorded on a XRD, PANalytical, X'PertPRO instrument with Cu-Kα (λ = 1.5406 Å) radiation. Raman spectra were recorded for the electrodes on a Bruker Senterra Dispersive Raman Microscope spectrometer; the laser excitation wavelength was fixed at 785 nm. XRD patterns of Sb_2S_3 nanorods and Raman spectra of neat PEDOP and PEDOT films and Sb_2S_3 are provided in ESI† (Fig. S1, S2 and Table S1). Atomic force microscopy (AFM) and conducting-AFM (C-AFM) measurements were performed on the electrodes using a Veeco, Multimode 8 with a ScanAsyst (Nanoscope 8.10 software) microscope. The conductive probes used in this study were coated with Pt–Ir on front and back sides. The probe tip had a radius of 10 nm, spring constant of 0.2 N cm^{-2}, a current sensitivity of 1 nA V^{-1} and a load force of 50 nN was maintained between the tip and the sample. The sample deposited on FTO coated glass (area ~ 9 mm^2) was affixed on a stainless steel disk with a conducting carbon tape. A thin strip of pin-hole free silver paste was used for making contacts. The C-AFM cantilever scans the surface while in contact and both the topography and the current flowing through the sample are imaged at the same time. A contact topography image is generated by using the feedback loop to maintain the constant tip deflection and the current image is generated by measuring the current flow. A 50 mV bias was applied to the tip during imaging. Surface morphology analysis was performed using a Carl Zeiss (Supra 40) field emission scanning electron microscope (FE-SEM). Galvanostatic charge–discharge measurements were performed using a battery testing unit (Arbin Instruments, BT 2000) at different current densities in the voltage range of 0 to +1.0 V for two-electrode cells. Specific capacitance (SC, F g^{-1}) was determined using the galvanostatic charge–discharge curves. Electropolymerization, cyclic voltammetry and electrochemical impedance spectra were recorded on an Autolab PGSTAT 302N equipped with NOVA 1.7 software.

3. Results and discussion

3.1. Topography of electrodes

AFM images of pristine Sb_2S_3 nanorods are shown in Fig. 1. The low magnification topographical images of neat Sb_2S_3 (Fig. 1a and c) reveal a three-dimensional network of interlinked but

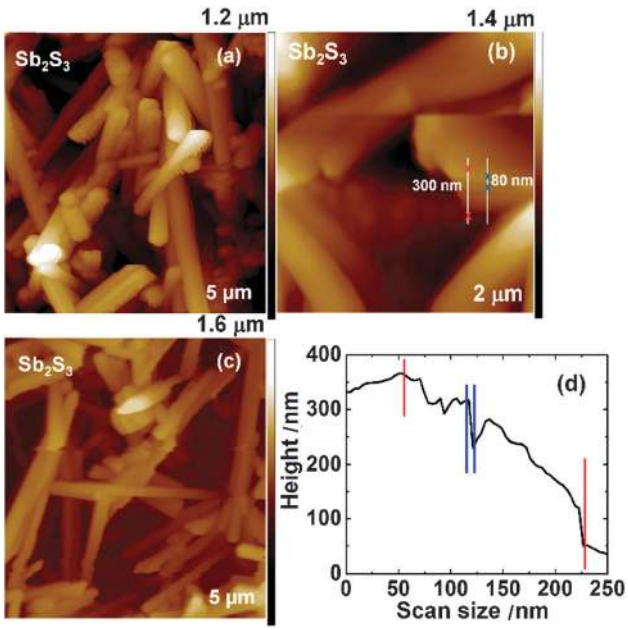

Fig. 1 Topography images of (a, c) Sb_2S_3 nanorods over different regions of the same film with scan sizes of 5 μm × 5 μm, (b) over a scan size of 2 μm × 2 μm and (d) a section profile of a stack of Sb_2S_3 nanorods from (b) showing the stack thickness of ~300 nm and an individual rod having a thickness of ~80 nm.

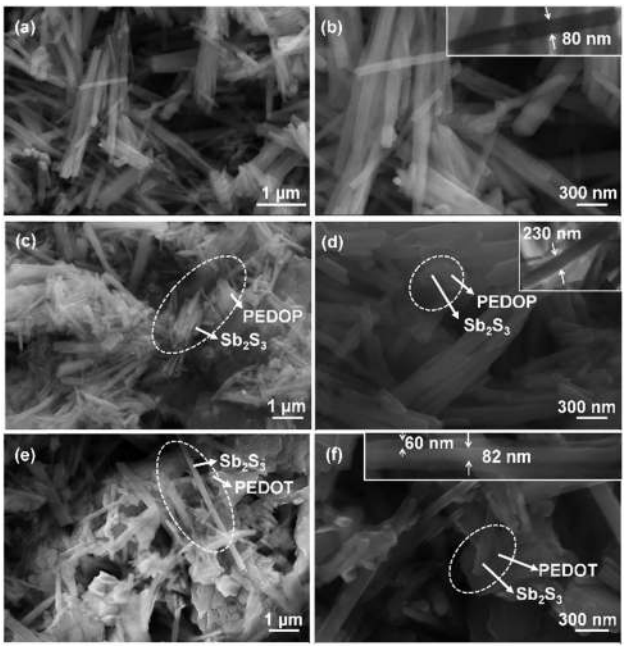

Fig. 2 FE-SEM images of (a, b) Sb_2S_3 nanorods, (c, d) PEDOP–Sb_2S_3 and (e, f) PEDOT–Sb_2S_3 films. Insets of (b, d and f) are enlarged high contrast images derived from the micrographs.

randomly oriented rods, with lengths varying from 1 to 3 μm and widths ranging from 50 to 150 nm. Since there are hardly any particulate shapes visible in the images, it is obvious that the synthetic process is quite efficient for producing homogenously distributed rectangular shaped nanorods. The high magnification image of pristine Sb_2S_3 nanorods shows that the rods have flattened surfaces and they tend to aggregate (Fig. 1b). The thickness of the rod, which was measured from a cross-sectional profile is approximately 80 nm and upon stacking the thickness increased to about 300 nm (Fig. 1d).

The SEM images of pristine Sb_2S_3 nanorods, shown in Fig. 2a and b, reveal the nanorods to be characterized by forest like growth, misaligned with respect to each other, but devoid of any branching. There are no particles or aggregates indicating that the sample is entirely made up of uniform nanorods having a smooth surface texture. The rods extend upto few microns in length and their diameters vary between 50 to 150 nm which concur with the AFM observations. The inset of Fig. 2b shows a high contrast image of the rod, and the rod width/thickness was 80 nm. The SEM images of the PEDOP–Sb_2S_3 composite (Fig. 2c and d) show the Sb_2S_3 nanorods to be juxtaposed with the PEDOP grains, indicating a good mixing of the polymer with the rods, the particulate sheath formed on the rods stem from the polymer. The inset of Fig. 2d shows the width of the rod to be 230 nm, which is greater than that of pristine Sb_2S_3 rods indicating the presence of a polymer around the rod. Further, it is also noticed that the pristine rods have sharp edges whereas upon integration with the polymer, their edges are jagged, indicative of polymer incorporation. This was observed in both composites. The SEM image of the PEDOT–Sb_2S_3 composite (Fig. 2e and f) shows the nanorods to be coated with the polymer. The high contrast inset in Fig. 2f shows a core Sb_2S_3 rod with a diameter of ~80 nm surrounded by a polymer sheath of approximately 60 nm thickness on either side, taking the total width to 200 nm. It is obvious that the inclusion of Sb_2S_3 nanorods in the polymer matrix affords high surface area to facilitate electrochemical reactions, in contrast to pristine PEDOP or PEDOT. The SEM images of PEDOP and PEDOT are shown in Fig. S2, ESI.† The pristine conducting polymer films have a granular morphology typical of electropolymerized conducting polymers.

3.2. XPS studies of electrodes

The survey spectra of the PEDOP–Sb_2S_3, PEDOT–Sb_2S_3 and pristine Sb_2S_3 films are shown in Fig. S5 (ESI†). Signals from C1s, Sb3d, P2p, F1s and S2p levels are common to the survey spectra of both PEDOP–Sb_2S_3 and PEDOT–Sb_2S_3, but the PEDOP–Sb_2S_3 film shows an additional signal from N1s. While the antimony and sulfur peaks indicate the inclusion of Sb_2S_3 quantum dots in the polymer matrix, the fluorine and phosphorous peaks imply the incorporation of the ionic liquid anion: $[(C_2F_5)_3(PF_3)]^-$ as the counter ion compensating the positive charge on the polymer (PEDOP or PEDOT) backbone. The deconvoluted C1s core level spectrum of PEDOP–Sb_2S_3 film (Fig. 3a) consists of four components at 284.6, 286, 289.2 and 290.8 eV, which can be attributed to C–C, C–N, C–O and C–F linkages respectively whereas the C1s spectrum of PEDOT–Sb_2S_3 (Fig. 4a) comprises of five peaks due to C–C, C–S, C–O, C–F and π–π* shake-up of the thiophene ring. The N1s profile observed for the PEDOP–Sb_2S_3 film (Fig. 3b) is asymmetric indicating that nitrogen prevails in two different chemical environments. The low energy peak at 399.5 eV arises from the –NH– bond of the pyrrole ring in the polymer and the high energy peak at 401.5 eV stems from the nitrogen of the 1-butyl-3-methyl imidazolium cation. The insertion of the imidazolium cation along with the trialkylphosphate (FAP) anion in the polymer film, during oxidative electropolymerization, is not unusual, as has been observed in the past by us for PEDOT films doped by ionic liquid functionalized graphene.[27] Since the charge on every

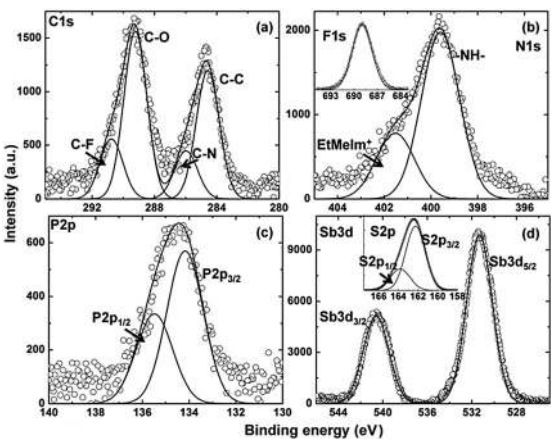

Fig. 3 Deconvoluted core level spectra of (a) C1s, (b) N1s, (c) P2p and (d) Sb3d of a PEDOP–Sb_2S_3 film. Insets of (b) and (d) are the F1s and S2p core level spectra.

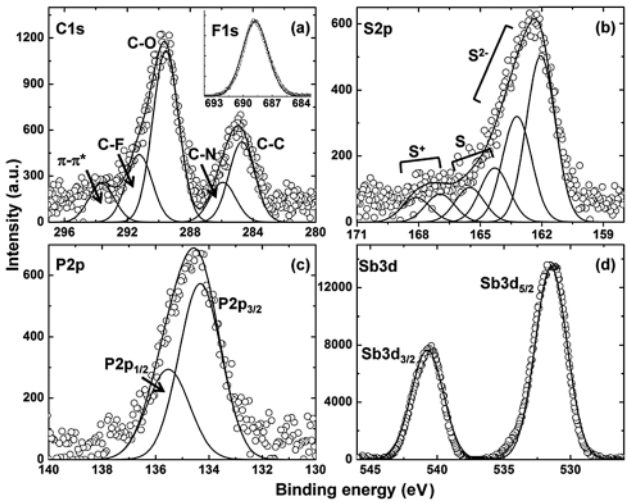

Fig. 4 Deconvoluted core level spectra of (a) C1s, (b) S2p, (c) P2p and (d) Sb3d of a PEDOT–Sb_2S_3 film. Inset of (a) shows a F1s core level spectrum.

imidazolium ion will be balanced by a charged FAP anion, the area under the $BuMeIm^+$ curve (denoted by I_{BuMeIm^+}) is a measure of the FAP counter-ion content in the polymer composite film. Therefore the ratio of $I_{BuMeIm^+}/I_{N(total)}$ represents the doping level in PEDOP by the ionic liquid. The value of this ratio is 0.28, which is the doping level in PEDOP by FAP ions. Our value is close to a value of 0.3 reported in the past for PEDOT films doped by poly(styrene sulfonate) or PSS.[28] The atomic ratio of $I_{C(total)}/I_{NH(pyrrole)}$ is ~7 for the PEDOP–Sb_2S_3 film, and is only slightly greater than the theoretical ratio of 6. A digression from the theoretical ratio of C : S, *i.e.* a value of 5 : 1 has been previously observed in films of PEDOT doped with dodecyl sulfate ions.[29] Authors attributed cause of deviation to the phase segregation of surfactant anions in the polymer surface region. The core-level spectrum of N1s was far too weak to extract reliable contribution from the imidazolium ion, in the PEDOT–Sb_2S_3 film. The deconvoluted P2p spectra for both PEDOP–Sb_2S_3 and PEDOT–Sb_2S_3 films (Fig. 3c and 4c) reveal two components at 135.5 and 134.2 eV due to the spin–orbit split, ascribable to $P2p_{1/2}$ and $P2p_{3/2}$ levels, and they originate from the PF_3 groups in the FAP anion.[30] These two films also show a single, intense, symmetric peak at ~689 nm arising from the F1s levels from the C–F and P–F bonds in the FAP anion. The twin peaks from Sb3d are clearly seen for both films (Fig. 3d and 4d), indicating the inclusion of Sb_2S_3 in the composites.

The S2p core level spectrum of PEDOP–Sb_2S_3 consists of two peaks corresponding to the spin-split doublet: $S2p_{1/2}$ and $S2p_{3/2}$ at 163.8 and 162.3 eV respectively with a relative intensity of 1 : 2 (inset of Fig. 3d). This doublet arises from sulfide in Sb_2S_3, as the polymer does not contain any sulfur. The S2p spectrum of PEDOT–Sb_2S_3 comprises of three sulfur doublets (Fig. 4b), the lowest energy pair at 162 and 163.2 eV originates from the sulfide ions (S^{2-}) in Sb_2S_3, the peak pair in the middle arises from neutral sulfur (–S–) of the thiophene rings in the polymer and the highest energy doublet arises from ionic sulfur ($-S^+=$) on the thiophene rings. The combined neutral and ionic sulfur contribution (arising only from PEDOT) and represented by ($I_S + I_S^+$) is deduced to be 0.34. The I_S^+ component is the measure of the anion content in the film, as every positively charged thiophene ring will be balanced by the FAP anion. We forgo the I_S^{2-} component as it arises only from Sb_2S_3, and does not contribute in any way to polymer doping. The ratio of $I_S^+/(I_S + I_S^+)$ is therefore expected to yield the doping level by FAP anion in this film, and it is deduced to be 0.37, which again is comparable to a value of 0.36 deduced from XPS studies on a PEDOT film doped with dodecyl sulfate ions.[31] Similarly, from the C1s spectrum of PEDOT–Sb_2S_3, the $I_{C(BuMeIm^+FAP)}/I_{C(PEDOP)}$ ratio, which signifies the only ionic liquid dopant to polymer sans dopant ratio, is found to be 0.369, which concurs well with the value obtained from the S2p data. Since the two values obtained from the deconvoluted data of two different core levels, *i.e.* S2p and C1s, are quite close, 0.37 is a reliable estimate of the doping level in the PEDOT film by FAP ions. The sulfide content in the PEDOT–Sb_2S_3 composite, denoted by $I_S^{2-}/I_{S(total)}$, is found to be 0.65; it involves contribution only from the sulfide in Sb_2S_3, and not from the polymer. This value is reasonably high, indicating that a high proportion of Sb_2S_3 prevails in the polymer. A crude estimate of the Sb_2S_3 content in PEDOP was also obtained from the ratio of the intensities of the split carbon peak's C–C component to the S2p peak (Fig. S5a, ESI†); the I_{S2p}/I_{C-C} was found to be 0.56.

3.3. Conducting-AFM studies on electrodes

Fig. 5 shows the topography and current images simultaneously recorded for identical regions of Sb_2S_3, PEDOP–Sb_2S_3 and PEDOT–Sb_2S_3 films; the scanned area was 5 μm × 5 μm for each film. The difference in the topography ongoing from Fig. 1 to 5 for

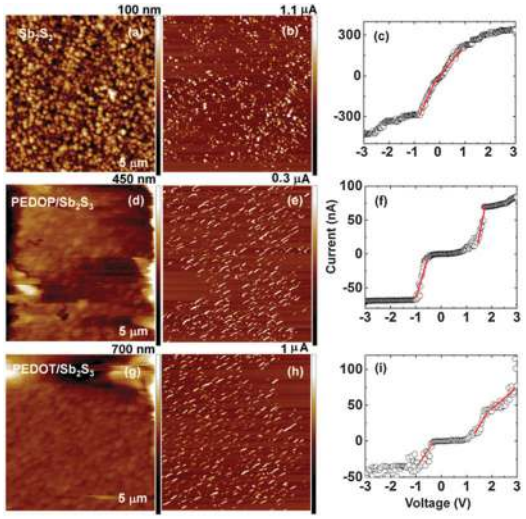

Fig. 5 Concurrent topography and current images of (a, b) Sb_2S_3 nanorods, (d, e) PEDOP–Sb_2S_3, (g, h) PEDOT–Sb_2S_3 films recorded over scanned areas of 5 μm × 5 μm. Resultant current-voltage curves of (c) Sb_2S_3 nanorods, (f) PEDOP–Sb_2S_3, (i) PEDOT–Sb_2S_3 films. Each curve is averaged over 15 *I*–*V* curves recorded at 15 spots on each current image shown in b, e and h.

the same samples (Sb_2S_3, PEDOP–Sb_2S_3 and PEDOT–Sb_2S_3) arises from the different modes used for making the measurement. While contact mode is used in C-AFM, tapping mode is used for recording conventional topography images (more details and the cross-sectional profiles (Fig. S6) are provided in ESI†). Here, the current images were generated by contacting a conductive tip with the film surface and a small bias voltage of 50 mV was applied between the tip and the substrate while the tip runs horizontally over the surface. In the current images, the bright regions are attributed to the high current flowing domains and the dark regions represent low currents. The current image of Sb_2S_3 nanorods shows uniformly distributed bright regions and an extraordinarily high current carrying capability, and the maximum current flowing through the film is 1.1 μA. The color-scale on the right side of the images provides a measure of the currents propagating in the films. The maximum currents neat PEDOP and PEDOT films are capable of carrying are 12 and 3.5 nA respectively and the number of high current bright domains are very sparse (Fig. S7b and d, ESI†). On incorporating Sb_2S_3 nanorods in the conducting polymer films, the current carrying capability of the polymers is considerably enhanced, which is also confirmed from the maximum currents of 0.05 and 1 μA observed in the current images of PEDOP–Sb_2S_3 and PEDOT–Sb_2S_3 respectively. In the neat polymer films, the current flow is poor as the films comprise of only localized spots of electron conduction, which are embedded in largely insulating regions. In the composites, on the other hand, the homogeneity of the bright regions, characteristic of high electron conductance is far superior to that in the corresponding neat films. The currents of the PEDOP–Sb_2S_3 and PEDOT–Sb_2S_3 films are 2 and 1000 times greater than that of neat PEDOP and PEDOT films, for the same value of applied bias. In the PEDOP–Sb_2S_3 and PEDOT–Sb_2S_3 films, the enwrapping of the Sb_2S_3 nanorods by the polymer chains occurs at the molecular level, due to the single step potentiostatic deposition from a plating sol containing both the monomer and the Sb_2S_3 nanorods. The polymer is in direct contact with the Sb_2S_3 nanorods, and therefore the flow of electrons through the bulk of the composite is facile as the Sb_2S_3 nanorods possess an intrinsic ability to conduct electrons. Such an unobstructed electron propagation through the bulk of the neat PEDOP or PEDOT films is not realized, as they are relatively almost electronically insulating.

In the neat PEDOP or PEDOT films, the high current spots/islands are embedded in large insulating domains as opposed to the composite PEDOP–Sb_2S_3 and PEDOT–Sb_2S_3 films, wherein the high current (bright) regions tend to dominate, thus improving the cross-sectional conduction of electrons in the film. The current section profile of the composite films (Fig. S6, ESI†) complements the imaging, as the span of crests corresponding to high currents is significantly wider than the (few) troughs corresponding to low currents. It is apparent that localized electron conduction is rather uniform across the composite films. The exactly opposite response was obtained for the neat films, as very few peaks corresponding to high currents were observed (Fig. S8, ESI†). Point contact *I–V* curves were recorded at fifteen equidistant points on each current image, and the average *I–V* profile for each film is shown (Fig. 5c, f and i). A quasi-linear dependence of current on swept potential was confined to narrow voltage windows. From the straight-line fits, within the voltage windows in which the *I–V* response was almost linear, ambient temperature electronic conductivities were determined by using eqn (1),

$$\sigma_{RT} = (I/V) \times (d/\pi r^2) \quad (1)$$

where r is the radius of the conducting tip and d is the thickness of the film. The average electronic conductivities for Sb_2S_3, PEDOP–Sb_2S_3 and PEDOT–Sb_2S_3 films were deduced from the ohmic regimes and were calculated to be 5, 1.735 and 1.01 S cm^{-1} respectively. The nanoscale conductivities of neat PEDOP and PEDOT were determined to be 0.053 and 0.068 S cm^{-1} respectively. The considerably enhanced average nanoscale conductivities of the composite films, 32 and 15 times greater than their neat counterparts, show that the Sb_2S_3 nanorods provide facile conduction pathways for electron movement and naturally enhance the conducting capacity of the polymer film.

3.4. Cyclic voltammetric studies

Fig. 6a and b show the comparison of cyclic voltammograms of neat films and their corresponding composites (PEDOP and PEDOP–Sb_2S_3 and PEDOT and PEDOT–Sb_2S_3), recorded at a constant scan rate of 50 mV s^{-1} in the potential range of 0 to +1 V. The CV profiles for PEDOT and PEDOT–Sb_2S_3 exhibit distinct rectangular shapes, indicating their capacitive nature. However, the area under the voltammogram is substantially higher for the composites compared to the neat polymer film, which implies a higher ion storage capacity for the former. The current density maxima with a plateau like span over a potential range of 0.1 to 1 V is 1.4 mA cm^{-2} for the composite as compared to 0.3 mA cm^{-2} for the neat polymer. A 5-fold increment in

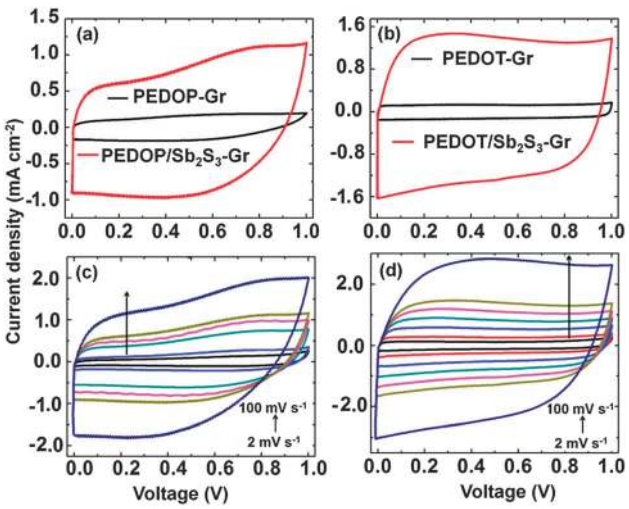

Fig. 6 Cyclic voltammograms of (a) PEDOP-Gr, PEDOP–Sb_2S_3-Gr devices, (b) PEDOT-Gr, PEDOT–Sb_2S_3-Gr cells compared by recording at the same scan rate of 100 mV s^{-1}, (c) PEDOP–Sb_2S_3-Gr and (d) PEDOT–Sb_2S_3-Gr cells at different scan rates of 2, 5, 10, 20, 50 and 100 mV s^{-1}.

current density ongoing from PEDOT to PEDOT–Sb_2S_3 is a clear indicator of the capability of Sb_2S_3 to uptake a greater amount of the conducting polymer, for the same geometric area. For the PEDOP–Sb_2S_3 composite, a quasi-rectangular voltammetric profile was observed, the slight undulations in the current density curve in the anodic scan is a consequence of oxidation of the polymer. The better accessibility of the electrolyte anions with PEDOT chains is afforded by the intertwined nanorods' morphology of Sb_2S_3. The polymer enwrapped Sb_2S_3 nanorods have interconnected elongated tubular morphologies, and the FAP or $[(C_2F_5)_3(PF_3)]^-$ ions from the electrolyte percolate more easily and have better access to the electroactive sites as compared to the pristine polymer. The neat polymers have granular compact morphologies, and therefore counter ion propagation through the film is not facile and as a consequence the ion storage capacity is lesser than that of the composites. It is also known that fast and efficient electron transfer from the electroactive film to the current collector enables a higher ion uptake from the electrolyte solution, and this is realized in the composite owing to the larger nanoscale electronic conductivities of the composites. The electrically conductive Sb_2S_3 nanorods are directly in contact with the PEDOP or PEDOT in the composites, which facilitate electron transport through the bulk of the composite and therefore improve the overall ion uptake capability of the electroactive electrode. Fig. 6c and d display the CV plots of the PEDOP–Sb_2S_3-Gr and PEDOT–Sb_2S_3-Gr based supercapacitor cells recorded at different scan rates. All the curves retain an almost rectangular shape, even at a high scan rate of 100 mV s^{-1}, which is characteristic of low contact resistance of the supercapacitor. A similar observation was made for a graphene hydrogel-MnO_2 based supercapacitor in a previous report.[32] The increase in the redox current as a function of scan rate, observed for the composite cells, is suggestive of good rate capability.

3.5. Charge–discharge characteristics of cells

The galvanostatic charge–discharge curves of PEDOP-Gr, PEDOP–Sb_2S_3-Gr, PEDOT-Gr and PEDOT–Sb_2S_3-Gr cells (obtained at a fixed current density of 1 A g^{-1} using a potential window of 0−1 V) are shown in Fig. 7a and b. All the four cells show a triangular shape, implying that the potential of charge or discharge varies linearly with time, which is indicative of good reversibility. The charge–discharge times vary for different electrodes, for a fixed value of applied current density, thus indicating different specific capacitances. The specific capacitance of the redox and redox composite based cells was calculated from the slope of the discharge curve and by using following equation.

$$C = i \times \Delta t/\Delta V \times m \qquad (2)$$

In eqn (2), C is the specific capacitance, i is the current applied for discharge, Δt is the time in seconds for discharge, ΔV is the voltage window and m is the mass of active material of the working electrode. The details of capacitance calculations are provided in ESI.† The specific capacitance for the PEDOP-Gr cell is 717 F g^{-1} in comparison to a SC of 1008 F g^{-1} achieved for the composite, at the same current density of 1 A g^{-1}.

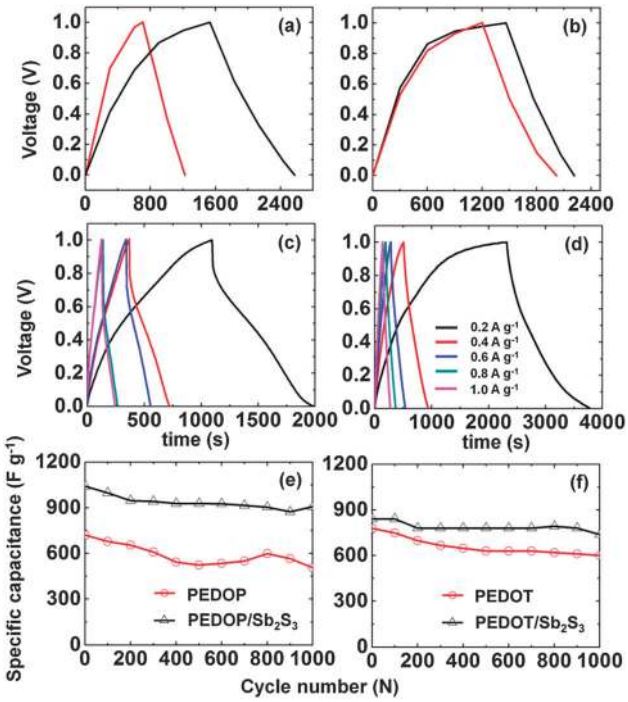

Fig. 7 Galvanostatic charge-discharge curves of (a) PEDOP-Gr, PEDOP–Sb_2S_3-Gr cells and (b) PEDOT-Gr, PEDOT–Sb_2S_3-Gr cells at a fixed current density of 1 A g^{-1}, rate capability of (c) PEDOP–Sb_2S_3-Gr and (d) PEDOT–Sb_2S_3-Gr cells (at different current densities of 0.2, 0.4, 0.6, 0.8, 1.0 A g^{-1}) and cycling performance of (e) PEDOP-Gr, PEDOP–Sb_2S_3-Gr and (f) PEDOT-Gr, PEDOT–Sb_2S_3-Gr cells at a fixed current density of 1 A g^{-1}.

Similarly, for the PEDOT–Sb_2S_3-Gr cell, it is 830 F g^{-1}, relative to 630 F g^{-1} for the cell based on the neat polymer. The large difference in specific capacitance ongoing from the neat polymer to the corresponding composite also points to the fact that the nanorods like morphology of Sb_2S_3 increases the anion intercalation capability of the polymer (by the virtue of large accessible surface area coated with the polymer). The higher accessible surface area to mass ratio achieved in the composites is responsible for the higher specific capacitances. The three-dimensional network of electrically conductive Sb_2S_3 nanorods serves as a scaffold for the conducting polymers in the composites. In a previous report, Liu *et al.* obtained a specific capacitance of 664 F g^{-1} for a composite PEDOT–RuO_2 hollow nanotube based cell.[12] In yet another study, a specific capacitance of 210 F g^{-1} was achieved for coaxial MnO_2–PEDOT nanowires.[13] Our values are comparable to literature values for conducting polymer nanostructured electrodes. The rate capability of the neat polymer and composite based cells was determined by recording the charge–discharge curves at different current densities of 0.2, 0.4, 0.6 and 1 A g^{-1} (Fig. 7c and d). The PEDOP–Sb_2S_3 composite retained 88% of its capacitance when the current density was increased from 0.2 to 1 A g^{-1}, thus indicating good rate performance. The rate performance of the neat polymer was abysmal, as the capacitance was only 630 F g^{-1} at a high current density of 1 A g^{-1}. The cycling stability of the PEDOP-Gr, PEDOP–Sb_2S_3-Gr, PEDOT-Gr and PEDOT–Sb_2S_3-Gr cells was also compared. The variation of

specific capacitance (obtained from the charge–discharge curves, at a current density of 1 A g^{-1}), as a function of galvanostatic charge–discharge cycles is shown in Fig. 7e and f. At the end of 1000 charge–discharge cycles, while the PEDOP–Sb_2S_3-Gr cell retained 87% of its initial capacitance, the corresponding neat polymer cell maintained only 70% of its original capacitance. The PEDOT–Sb_2S_3 cell also exhibited improved capacitance retention compared to the neat PEDOT cell. Sb_2S_3 nanorods furnish a robust support for the conducting polymers which prevents the polymer from swelling and shrinking during repetitive electrochemical cycling. This advantage is not realized in the cells based on neat polymers, and as a result, their capacitance decreases more steeply with cycling.

3.6. Electrochemical impedance spectroscopy

The Nyquist plots of PEDOP-Gr, PEDOP–Sb_2S_3-Gr, PEDOT-Gr and PEDOT–Sb_2S_3-Gr cells recorded under an ac perturbation signal of 0.1 mV, in the frequency range of 0.01 to 1M Hz, are shown in Fig. 8 and the related parameters are summarized in Table S2 (ESI†). Almost all the plots are composed of an arc followed by an inclined straight line. The undefined semicircle involves a parallel combination of interfacial resistance due to charge transfer (R_{CT}) and the corresponding electrical double layer capacitance (C_{dl}). The span of this arc is extremely small for both PEDOP–Sb_2S_3 and PEDOT-Gr composites as compared to the neat polymer. This indicates that the charge transfer resistance is small and the redox system is kinetically fast. The R_{CT} values are 296 Ω for PEDOP and 55 Ω for the PEDOP–Sb_2S_3 composite. The lower values of R_{CT} for both composites show that electron transfer from the composite to the underlying FTO electrode accompanied by anion transfer from the electrolyte to the composite is more facile relative to their rates in the neat PEDOP or PEDOT based cells. In the composite, the polymer coated Sb_2S_3 nanorods allow more number of electrolyte ions to access redox active sites on the polymer easily. In the low frequency regime, the impedance plot increases steeply and becomes almost vertical for all the four electrodes, characteristic of pure capacitive behavior. The extrapolation of the straight line yields the *x*-axis intercept which is equal to R_s + 1/3 R_Σ, where R_s is the uncompensated electrolyte resistance and R_Σ stands for the ion diffusion resistance or an internal resistance (characteristic of the electrode material). The ion diffusion resistance was 240 and 9 Ω for the PEDOP and PEDOP–Sb_2S_3 composites and 18 and 3 Ω for the PEDOT and PEDOT–Sb_2S_3 composites. This implies that after the counterions are transferred from the bulk gel electrolyte to the PEDOP–Sb_2S_3 composite, ions can easily diffuse through this electrode comprising of the three-dimensional network of polymer coated nanorods as compared to the neat electrode wherein ion-transport is hindered by the low electronic conductivity and also by the granular morphology. The EIS results reveal that the composites offer low resistance to ion diffusion in the electroactive phase and also to ion transfer at the electrolyte/film interface. The low internal resistance for both electron and ion-movement in the PEDOP–Sb_2S_3-Gr and PEDOT–Sb_2S_3-Gr composite based cells is responsible for the high capacitances attained by these cells even at a high charge–discharge rate. The fibrillar structures that prevail in the composite films afford short diffusion pathways thus improving the ion-transport properties of the composites. Such effects are not realized in the cells based on the neat PEDOP or PEDOT films and therefore the electrochemical performances are poor. The impedance plots for the PEDOP–Sb_2S_3-Gr and PEDOT–Sb_2S_3-Gr cells before and after cycling have been compared in Fig. 8c and d. After 1000 cycles, both ion-diffusion resistance and charge transfer resistance increase slightly, which is a manifestation of polymer swelling and shrinking upon repeated ion intercalation and de-intercalation.

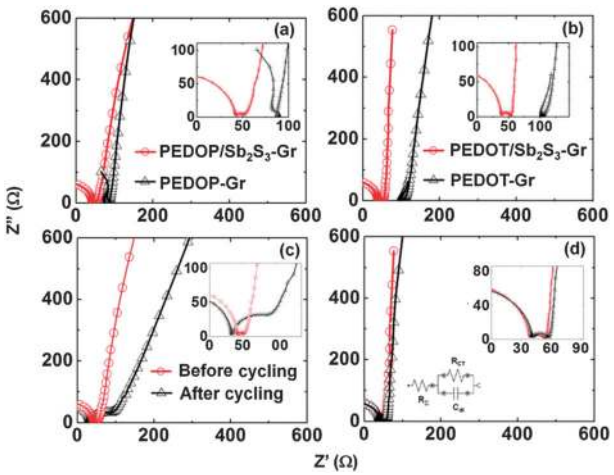

Fig. 8 Nyquist plots of (a) PEDOP-Gr, PEDOP–Sb_2S_3-Gr and (b) PEDOT-Gr, PEDOT–Sb_2S_3-Gr cells, comparison of Z″ *versus* Z′ plots before and after 1000 charge–discharge cycles of the composite based cells: (c) PEDOP–Sb_2S_3-Gr and (d) PEDOT–Sb_2S_3-Gr; all plots recorded in the frequency range of 0.01 Hz to 1 MHz. Corresponding insets show enlarged views of the same plots in the high frequency region. Inset of (d) shows the equivalent circuit used for fitting the experimental data.

3.7. Flexible supercapacitor

The performance characteristics of the conducting polymer–Sb_2S_3 composites motivated us to fabricate lightweight, flexible supercapacitors, using a carbon fiber cloth (sheet resistance ~2.7 Ω cm^{-2}, thickness ~3 mm, weight ~1.8 g cm^{-2}) instead of FTO coated glass. The cell was constructed with the following configuration: carbon fiber cloth/PEDOP/Sb_2S_3-EtMeIm$^+$ $[(C_2F_5)_3(PF_3)]^-$/PMMA gel-Gr/carbon fiber cloth, wherein, the graphite layer was electrophoretically deposited and the PEDOP–Sb_2S_3 composite was electropolymerized onto carbon fiber cloths. The galvanostatic charge–discharge plot recorded at a current density of 1 A g^{-1} and the cyclic voltammetric plot of the cell recorded at 50 mV s^{-1} are shown in Fig. 9. The specific capacitance was determined to be 150 F g^{-1}, which is comparable to the capacitance (150 F g^{-1} at 1 A g^{-1}) achieved for a flexible PEDOT based cell in a previous report.[33] In the cyclic voltammogram of the flexible device there is a steep curve at the extreme end from 0.9 V to 1 V. This is probably due to the

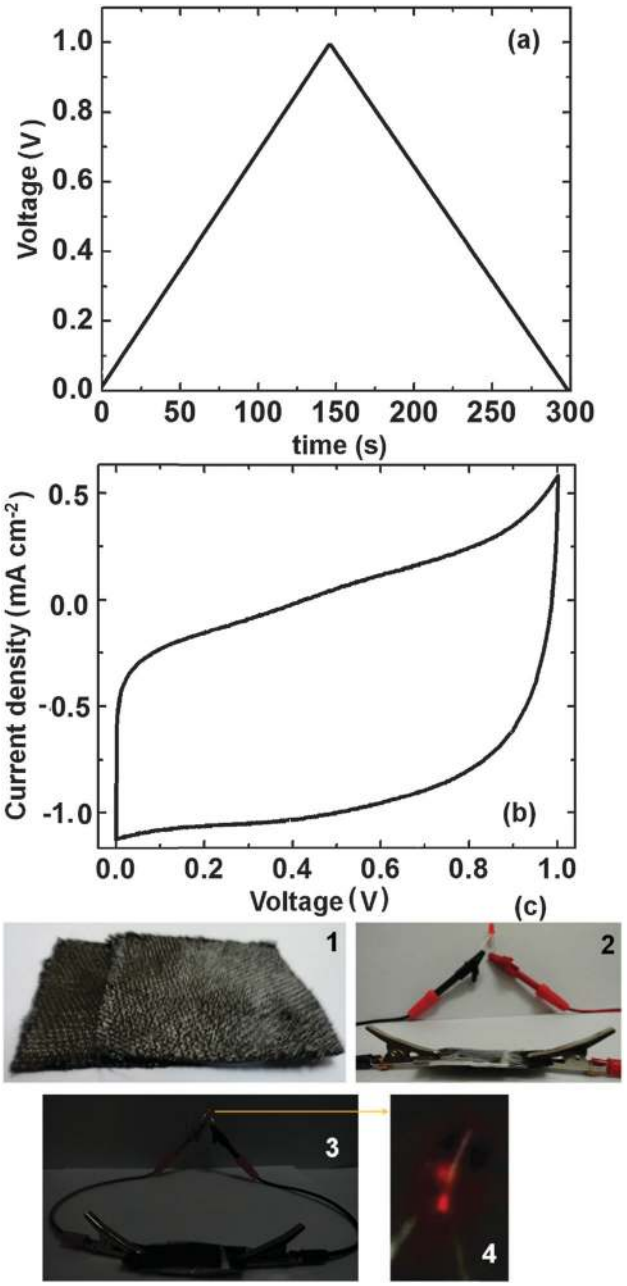

Fig. 9 (a) Charge–discharge curve recorded at a current density of 1 A g^{-1} and (b) cyclic voltammogram (at 10 mV s^{-1}) of a flexible, thin quasi solid-state supercapacitor cell with the following configuration: Carbon fiber cloth/PEDOP/Sb_2S_3-gel electrolyte-Gr/Carbon fiber cloth. (c) Photographs of (1) a flexible cell and (2–4) a LED illuminated by the flexible cell.

over oxidation and side reactions of the carbon fiber electrode. A LED was also illuminated with this cell.

4. Conclusions

Sb_2S_3 nanorods, extending in length to a few microns and 50–150 nm in width, and possessing unusually large bulk and nanoscale electronic conductivities, were prepared by a hydrothermal method in a pre-step. PEDOP–Sb_2S_3 and PEDOT–Sb_2S_3 composite electrodes were electro-synthesized from a monomer-Sb_2S_3 nanorod suspension. The enwrapping of Sb_2S_3 nanorods by PEDOP and PEDOT in the composites was ascertained by XPS and Raman studies, as high proportions of sulfide (greater than 0.5) in the composites were deduced from atomic ratios. The high surface area afforded by the Sb_2S_3 nanorods steers the formation of PEDOP–Sb_2S_3 and PEDOT–Sb_2S_3 composites with fibrillar structures which are strikingly different from the conventional granular morphologies achieved for the neat PEDOP and PEDOT films. Conducting-AFM analyses also showed the presence of a large number of uniformly distributed high current domains in the composites in contrast to the neat polymers for which sparsely distributed high current spots embedded in largely insulating regions, spanning over a few microns were observed. Further evidence for the effectiveness of Sb_2S_3 in serving as a three dimensional conductive scaffold was obtained in terms of nanoscale conductivities of the PEDOP–Sb_2S_3 and PEDOT–Sb_2S_3 composites which were 32 and 15 times higher in comparison to that obtained for the neat polymers. The role of Sb_2S_3 nanorods in greatly improving the ion uptake capability of PEDOP and PEDOT was reflected in the large specific capacitances of 1008 and 830 F g^{-1} (at 1 A g^{-1}), good rate capability and repetitive cycling durability (88 and 85% capacitance retention after 1000 cycles) for asymmetric supercapacitors constructed with the composite and graphite as the electrodes. The greatly enhanced power densities of the PEDOP–Sb_2S_3 and PEDOT–Sb_2S_3 composite supercapacitors (504 and 415 W kg^{-1}), relative to 315 and 350 W kg^{-1} for neat PEDOP and PEDOP cells are attributed to the fast charge–discharge rates effected by the lower ion-diffusion resistances offered by the composites. A practical demonstration of a LED illumination by use of a thin, lightweight, flexible supercapacitor constructed with PEDOP–Sb_2S_3 and graphite as the electroactive materials and a carbon-fiber cloth as the current collector opens up possibilities for using this inexpensive facile approach for creating composites of conductive Sb_2S_3 nanorods with a plethora of other conducting polymers as well for high performance supercapacitors.

Acknowledgements

Financial support from the Department of Science and Technology (SR/S1/PC-06/2010) is gratefully acknowledged.

Notes and references

1 M. E. Roberts, D. R. Wheeler, B. B. McKenzie and B. C. Bunker, *J. Mater. Chem.*, 2009, **19**, 6977–6979.
2 X. Zhao, B. M. Sanchez, P. J. Dobson and P. S. Grant, *Nanoscale*, 2011, **3**, 839–855.
3 C. H. Lai, M. Y. Lu and L. Chen, *J. Mater. Chem.*, 2012, **22**, 19–30.
4 C. Tang, K. Hackenberg, Q. Fu, P. M. Ajayan and H. Ardebili, *Nano Lett.*, 2012, **22**, 1152–1156.
5 Y. Xia, K. Sun and J. Ouyang, *Adv. Mater.*, 2012, **24**, 2436–2440.

6 H. Lee, J. K. Yoo, J. H. Park, J. H. Kim, K. Kang and Y. S. Jung, *Adv. Mater.*, 2012, **2**, 976–982.
7 L. Dai, D. W. Chang, J. B. Baek and W. Lu, *Small*, 2012, **8**, 1130–1166.
8 S. A. Hashmi, A. Kumar and S. K. Tripathi, *Eur. Polym. J.*, 2005, **41**, 1373–1379.
9 K. Zhang, L. L. Zhang, X. S. Zhao and J. Wu, *Chem. Mater.*, 2010, **22**, 1392–1401.
10 C. Peng, S. Zhang, D. Jewell and G. Z. Chen, *Prog. Nat. Sci.*, 2008, **18**, 777–788.
11 L. Yang, S. Cheng, Y. Ding, X. Zhu, Z. L. Wang and M. Liu, *Nano Lett.*, 2012, **12**, 321–325.
12 R. Liu, J. Duay, T. Lane and S. B. Lee, *Phys. Chem. Chem. Phys.*, 2010, **12**, 4309–4316.
13 R. Liu and S. B. Lee, *J. Am. Chem. Soc.*, 2008, **10**, 2942–2943.
14 R. B. Rakhi, W. Chen, D. Cha and H. N. Alshareef, *Nano Lett.*, 2012, **5**, 2559–2567.
15 Q. Qu, Y. Zhu, X. Gao and Y. Wu, *Adv. Energy Mater.*, 2012, **2**, 950–955.
16 M. S. Wu, Y. P. Lin, C. H. Lin and J. T. Lee, *J. Mater. Chem.*, 2012, **22**, 2442–2448.
17 J. Han, L. Li, P. Fang and R. Guo, *J. Phys. Chem. C*, 2012, **116**, 15900–15907.
18 C. Meng, C. Liu, L. Chen, C. Hu and S. Fan, *Nano Lett.*, 2010, **10**, 4025–4031.
19 M. Ertas, R. M. Walczak, R. K. Das, A. G. Rinzler and J. R. Reynolds, *Chem. Mater.*, 2012, **3**, 433–443.
20 A. Davies, P. Audette, B. Farrow, F. Hassan, Z. Chen, J. Y. Choi and A. Yu, *J. Phys. Chem. C*, 2011, **35**, 17612–17620.
21 S. Cho and S. B. Lee, *Acc. Chem. Res.*, 2008, **6**, 699–707.
22 A. Kumar and J. R. Reynolds, *Macromolecules*, 1996, **29**, 7629–7630.
23 C. L. Gaupp, K. Zong, P. Schottland, B. C. Thompson, C. A. Thomas and J. R. Reynolds, *Macromolecules*, 2000, **33**, 1132–1133.
24 B. N. Reddy, M. Deepa, A. G. Joshi and A. K. Srivastava, *J. Phys. Chem. C*, 2011, **115**, 18354–18365.
25 B. N. Reddy and M. Deepa, *Electrochim. Acta*, 2012, **70**, 228–240.
26 T. H. Perez, M. Morales, N. Batina and M. Salmona, *J. Electrochem. Soc.*, 2001, **5**, 369–375.
27 A. P. Saxena, M. Deepa, A. G. Joshi, S. Bhandari and A. K. Srivastava, *ACS Appl. Mater. Interfaces*, 2011, **3**, 1115–1126.
28 J. Hwang, F. Amy and A. Kahn, *Org. Electron.*, 2006, **7**, 387–396.
29 N. Sakmeche, S. Aeiyach, J. J. Aaron, M. Jouini, J. C. Lacroix and P. C. Lacaze, *Langmuir*, 1999, **15**, 2566–2574.
30 I. Niedermaie, C. Kolbeck, N. Taccardi, P. S. Schulz, J. Li, T. Drewello, P. Wasserscheid, H. P. Steinrück and F. Maier, *ChemPhysChem*, 2012, **13**, 1725–1735.
31 C. Li and T. Imae, *Macromolecules*, 2004, **7**, 2411–2416.
32 H. Gao, F. Xiao, C. B. Ching and H. Duan, *ACS Appl. Mater. Interfaces*, 2012, **5**, 2801–2810.
33 S. Cho, D. H. Choi, S. H. Kim and S. B. Lee, *Chem. Mater.*, 2005, **17**, 4564–4566.